LIMNOLOGY
and
OCEANOGRAPHY

ASLO

Limnol. Oceanogr. 9999, 2020, 1–15

doi: 10.1002/lno.11400

A novel cross-shore transport mechanism revealed by subsurface, robotic larval mimics: Internal wave deformation of the background velocity field

Jessica C. Garwood,[1*] **Andrew J. Lucas**,[1,2] **Perry Naughton**,[3] **Matthew H. Alford**,[1] **Paul L. D. Roberts**,[1,4] **Jules S. Jaffe**,[1] **Laura deGelleke**,[5] **Peter J. S. Franks**[1]

[1]Scripps Institution of Oceanography, UCSD, La Jolla, California
[2]Department of Mechanical and Aerospace Engineering, UCSD, La Jolla, California
[3]Department of Electrical and Computer Engineering, UCSD, La Jolla, California
[4]Monterey Bay Aquarium Research Institute, Moss Landing, California
[5]Department of Oceanography, Dalhousie University, Halifax, Nova Scotia, Canada

Abstract

Coastal physical processes are essential for the cross-shore transport of meroplanktonic larvae to their benthic adult habitats. To investigate these processes, we released a swarm of novel, trackable, subsurface vehicles, the Mini-Autonomous Underwater Explorer (M-AUEs), which we programmed to mimic larval depth-keeping behavior. The M-AUE swarm measured a sudden net onshore transport of 30–70 m over 15–20 min, which we investigated in detail. Here, we describe a novel transport mechanism of depth-keeping plankton revealed by these observations. In situ measurements and models showed that, as a weakly nonlinear internal wave propagated through the swarm, it deformed surface-intensified, along-isopycnal background velocities downward, accelerating depth-keeping organisms onshore. These higher velocities increased both the depth-keepers' residence time in the wave and total cross-shore displacement, leading to wave-induced transports twice those of fully Lagrangian organisms and four times those associated with the unperturbed background currents. Our analyses also show that integrating velocity time series from virtual larvae or mimics moving with the flow yields both larger and more accurate transport estimates than integrating velocity time series obtained at a point (Eulerian). The increased cross-shore transport of organisms capable of vertical swimming in this wave/background-current system is mathematically analogous to the increase in onshore transport associated with horizontal swimming in highly nonlinear internal waves. However, the mechanism described here requires much weaker swimming speeds (mm s^{-1} vs. cm s^{-1}) to achieve significant onshore transports, and meroplanktonic larvae only need to orient themselves vertically, not horizontally.

Meroplanktonic larvae of coastal benthic organisms, such as barnacles, mussels, and oysters, must either remain in or be transported back to the nearshore environment for recruitment to adult populations. Simple hydrodynamic models that assume larvae to be completely passive and vulnerable to ocean currents tend to overestimate dispersal distances, both in the cross-shore and alongshore directions, when compared to estimates inferred from in situ larval abundance (Largier 2003; Shanks 2009). Accounting for simple behaviors such as vertical swimming can reconcile some of these estimates (Shanks and Brink 2005). By regulating their depths, for instance, organisms can exploit vertical variations in cross-shore velocities (Peterson et al. 1979; Morgan et al. 2009), or limit offshore transport (Shanks and Brink 2005). Such physical-biological interactions have been suggested to occur in internal gravity waves (Shanks and Wright 1987; Pineda 1999). However, less attention has been focused on the implications of internal waves interacting with depth-varying background flows for the transport of depth-keeping organisms.

As they propagate through a stratified ocean, internal waves deform isopycnal surfaces. Because background currents flow mainly along isopycnals, internal waves similarly deform the background velocity field, and more precisely its streamlines (Stastna and Lamb 2002; Klymak et al. 2006). Using measurements collected by a swarm of novel, subsurface larval mimics, the Mini-Autonomous Underwater Explorers (M-AUEs) (Jaffe et al. 2017), combined with simple models, we

*Correspondence: jgarwood@ucsd.edu

will show that this deformation has a significant impact on the transport of depth-keeping vs. passive larvae, particularly when the background horizontal currents are vertically sheared. To avoid any ambiguity associated with the term Lagrangian, we use the terms "passive" to refer to fully Lagrangian organisms, that are organisms that are advected by both horizontal and vertical velocities, and "depth-keeping" for organisms that are advected by horizontal velocities, but which resist vertical velocities.

Shanks (1983) demonstrated the potential of internal waves to transport plankton by deploying drifters in visible surface slicks—the surface expression of internal waves. Although the surface drifters occasionally showed no net horizontal displacement, at other times they were displaced as much as 1–2 km onshore in a few hours. Since then, a number of field studies have shown plankton and larvae to be concentrated above internal wave troughs (e.g., Shanks and Wright 1987; Pineda 1999; Lennert-Cody and Franks 2002; Omand et al. 2011), and theoretical arguments have shown the potential for internal waves to both accumulate (Franks 1997; Lennert-Cody and Franks 1999; Jaffe et al. 2017) and transport (Lamb 1997; Helfrich and Pineda 2003; Scotti and Pineda 2007) organisms with vertical swimming behaviors. Planktonic larvae have been shown to respond to a number of environmental cues that could orient them vertically—a necessary condition for these physical-biological interactions to occur. Scallop larvae, for instance, exhibit negative geotaxis and swim faster with increased pressure (Cragg 1980), while other invertebrate larvae aggregate in surface or bottom waters based on water temperature and stratification (Daigle and Metaxas 2011). Gastropod and oyster larvae sink or actively dive when encountering turbulence (Fuchs et al. 2004, 2013), a behavior that has been suggested to increase shoreward transport in the surf zone (Fujimura et al. 2014; Morgan et al. 2017).

The timing and strength of internal waves, including the internal tide, can be highly variable due to interactions with background stratification and velocities (e.g., Nash et al. 2012). Nonetheless, internal waves with frequency on the order of the local buoyancy are common in stratified, shallow coastal waters, where waves are refracted by the sloping bathymetry and propagate largely in the onshore direction (incidence angles $< 25°$) (Richards et al. 2013; Colosi et al. 2018; Sinnett et al. 2018).

Many studies have focused on internal-wave transport of water parcels; these results can be applied to passive organisms, but not to swimming organisms (e.g., Wunsch 1971; van den Bremer et al. 2019; but note the exceptions of Dewar 1980 and Franks et al. In press). Using linear wave theory in the absence of background flows, Franks et al. (In press) showed that both the direction and magnitude of transport experienced by passive and swimming organisms in internal waves depended on the organism's depth and vertical swimming ability. Sinusoidal, linear internal waves alone, however, are not expected to induce significant net transport of organisms: positive horizontal velocities are matched in magnitude by negative velocities, and integrate to zero at a fixed depth. In these linear waves, any net transport can thus be attributed to Stokes drift (Thorpe 1968; Dewar 1980), which tends to be weak.

Unlike linear internal waves, the wave velocities associated with highly nonlinear internal waves of depression are both larger in magnitude as well as persistently in the direction of the wave's propagation at the surface, that is, onshore for onshore-propagating waves, and negative/offshore at depth (Apel et al. 1985). The associated surface transports are thus expected to be greater than transports due to linear internal waves, particularly because the large isopycnal depressions drive strong surface velocities (e.g., Lamb 1997). For instance, surface transport distances calculated for nonlinear internal wave packets on the New Jersey shelf averaged to 1–2 km, but reached as much as 10 km for a particularly large-amplitude wave event (Shroyer et al. 2010). On other continental shelves, nonlinear internal waves have been found to account for sustained horizontal transports of 0.2–0.5 $m^2\ s^{-1}$ integrated over the surface layer (Inall et al. 2001; Zhang et al. 2015).

High densities of larvae of benthic organisms can be found within ~ 5 km of the coast (e.g., Shanks and Brink 2005; Morgan et al. 2009), suggesting that internal-wave-induced transport could return surface larvae to the nearshore habitat and maintain recruitment in some populations. Translating internal-wave-induced transport estimates to studies of larval displacement directly, however, is challenging because (1) estimates often focus only on wave-induced transport, not total transport, (2) the methodologies are based on passive water parcels, not swimming organisms, and (3) estimates are typically Eulerian and not along an organism's path.

To assess the total transport associated with an impinging internal wave, both the background currents and planktonic swimming must be taken into account, as they modify the residence time of organisms in a wave (Shanks 1995; Lamb 1997; Pineda 1999). Internal waves and background currents, however, do not act independently: during their passage, internal waves deform the vertical structure of background currents (Stastna and Lamb 2002; Klymak et al. 2006), while background currents modify the shape of internal waves and affect their propagation speeds.

Here, we focus on describing a novel cross-shore transport mechanism specific to depth-keeping organisms. This mechanism was revealed by the 3-D, underwater positions collected in situ by our larval mimics as they encountered a weakly nonlinear internal wave. Using data analyses and simple wave models, we show that the sudden increase in the mimic's cross-shore transport can be explained by the deformation of surface-intensified, onshore-flowing waters downward to the depths of the mimics. We also demonstrate that the internal wave deformation of vertically sheared background flows will influence the transport of depth-keeping organisms, but not

that of non-motile organisms. Thus, where internal waves deform an onshore-flowing surface layer downward, depth-keeping has the potential to increase onshore transport of larvae, potentially aiding their recruitment to suitable nearshore habitats.

Materials and methods

Field site

Experiments were conducted in June 2016 using small boats within 3 km of Mission Beach, California (Fig. 1). The coastline at Mission Beach roughly aligns in the north–south direction, and the shelf bathymetry is smooth and shore-parallel. The uniform alongshore bathymetry facilitates comparisons with simple 2-D internal wave models. These characteristics, and the proximity to Scripps Institution of Oceanography, have led to the use of the region as an internal wave laboratory for more than 50 yr (Armstrong and LaFond 1966).

Deployments targeted water depths < 30 m where trains of onshore propagating internal waves have been previously observed (Lerczak 2000; Lucas et al. 2011*a*). Given the local quasi-two-layer stratification, high-frequency internal wave trains have properties that agree well with linear theory, with phase speeds on the order of 10–20 cm s^{-1} (Lerczak 2000). The present study took place in similar conditions to previous experiments in the region.

Larval mimics

The M-AUEs are novel subsurface vehicles designed to mimic larvae and other plankton (Fig. 2a): they are small (1.5 L) and can be programmed with vertical swimming behaviors (Jaffe et al. 2017). Because the vehicles' 3D underwater positions can be determined on spatial scales of meters and temporal scales of tens of seconds, the M-AUEs are ideal for studying biological implications of high-frequency physical processes. To control their vertical positions, the M-AUEs use small piston adjustments to regulate their buoyancy relative to a target pressure/depth (Jaffe et al. 2017). The vehicles are equipped with pressure and temperature sensors to characterize their physical environment, an internal clock, and a hydrophone to record acoustic ranging pings emitted by a moored array of surface buoys.

In the present instance, the M-AUEs were programmed to maintain an approximately constant depth to simulate the tendency of some larvae to swim against vertical velocities, as inferred from cross-shore concentration surveys (Shanks and Brink 2005), and confirmed by tracking individual plankters both in situ (Genin et al. 2005) and in a laboratory flume (DiBacco et al. 2011). Seven plankton mimics were deployed for approximately 2 h near the surface (3-m target depth), where internal-wave-induced horizontal currents were expected to be large. To ensure the M-AUEs were above the pycnocline, the target depth was selected immediately prior to deployment based on real-time water column data transmitted via cellular network every 20 min from a moored, profiling Wirewalker (Rainville and Pinkel 2001; Pinkel et al. 2011; Lucas et al. 2011*a*). We focus here on the analysis of one particularly well-resolved wave event on the afternoon of 27 June 2016.

Pinger array

The underwater positions of the M-AUEs were estimated using time-of-flight measurements of acoustic pings from a

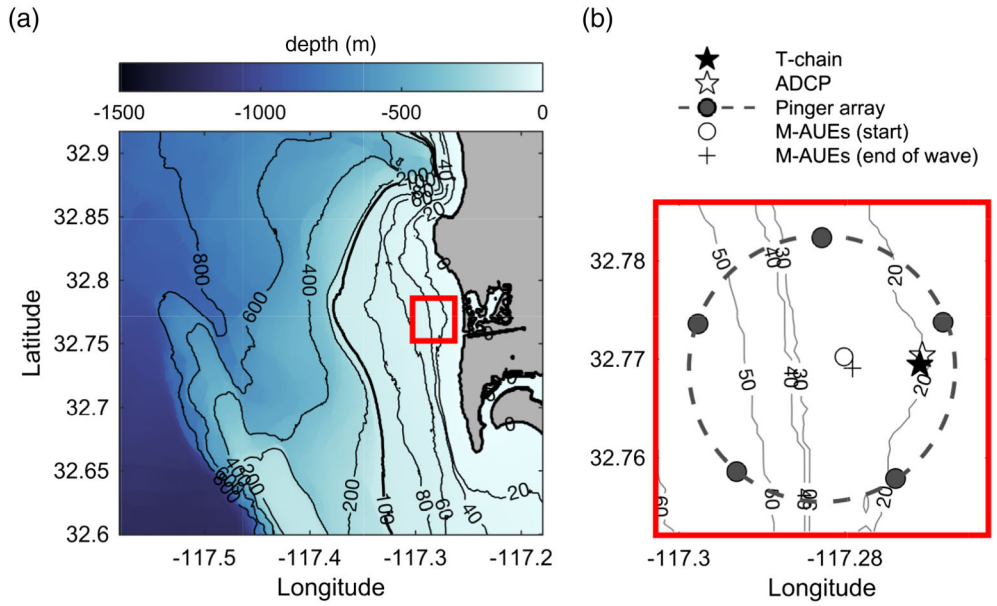

Fig. 1. Map of field site. (**a**) Bathymetric contours at every 20 m (0–100 m depth) and at every 200 m (> 100 m depth). Red box shows location of inset (**b**). (**b**) Bathymetric contours at every 10 m are shown, as well as locations of the T-chain, ADCP, pingers, and mean M-AUE start and end positions for the wave event described in this study.

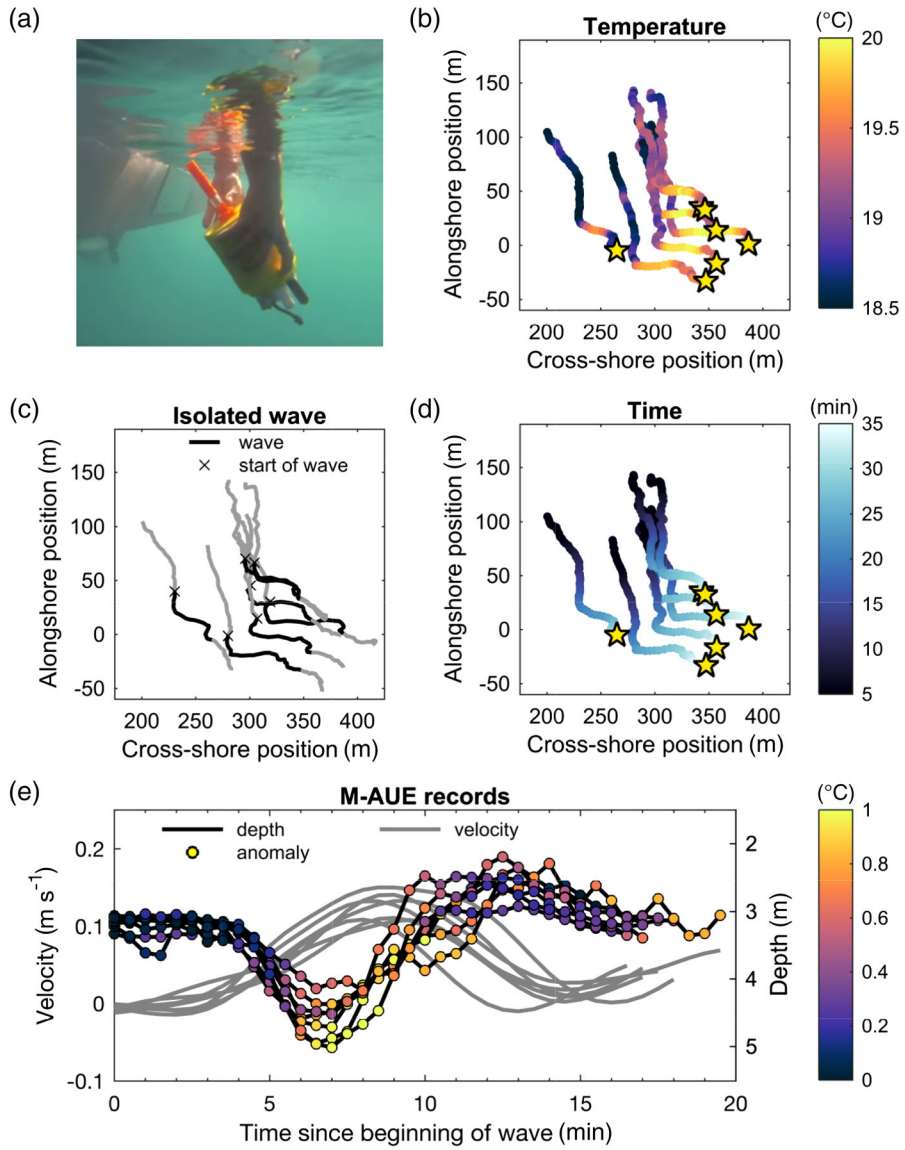

Fig. 2. M-AUE deployment on the afternoon of 27 June 2016. (**a**) Underwater picture of one M-AUE being deployed from a small boat. (**b**) M-AUE tracks, with color showing the temperature (°C) recorded by each vehicle. Stars show the location of the M-AUEs at the end of the wave of interest. (**c**) M-AUE tracks showing the wave event isolated for this study in black. Black "Xs" show the start of the wave. (**d**) Same as (**b**), but color shows time since the start of the deployment (min). (**e**) Vertical displacement (m) (right axis), temperature anomaly (°C) relative to temperature recorded at the start of the wave, and smoothed cross-shore velocities (m s^{-1}) (left axis) experienced by the M-AUEs during the wave event highlighted. Time is shown from when the wave first reached each M-AUE, shown by the black "Xs" in (**c**).

moored pinger array (Jaffe et al. 2017). Five acoustic pingers were mounted just below the water surface on separate moorings, each with continuous GPS navigation (Fig. 1). The pentagonal pinger array spanned isobaths from 10 to 50 m, and was about 3 km in diameter. Each pinger emitted a GPS-time-scheduled ping every 12 s, and pings between adjacent pingers were separated by 2 s; there was a pause of 4 s between each five-ping sequence (Jaffe et al. 2017). The horizontal positions of the M-AUEs deployed inside the pinger array were then calculated postdeployment by trilateration, using the time delays between ping emission and its recorded arrival time at the M-AUE (Jaffe et al. 2017). Under optimal conditions, the horizontal position of each M-AUE could be obtained every 12 s. However, the noise from the M-AUE piston motor occasionally obscured the recorded ping, reducing the temporal resolution of the M-AUE navigation. Keeping only the sequences for which all five pings were properly recorded resulted in successful localizations every 12 s more than 50% of the time. Overall, vehicles were located on average every 19–25 s, so their positions were interpolated to a common time vector with

30-s time intervals. Vehicle velocities were derived from the tracks, and smoothed with a LOESS filter (Cleveland and Grosse 1991) and a 12.5-min window. The precision of the position estimates varied from one vehicle to the other and depended on sea state, but using an error of ± 5 m horizontally encompassed > 95% of the residuals in estimated distance from each pinger, based on a test deployment that presented more localization issues (not shown). Residuals were calculated by subtracting the distances between each pinger and vehicle, estimated by trilateration, from the distances calculated using the time delays. The 2-h duration of the M-AUE swarm deployment was set by the time it took the M-AUEs to drift out of the 3-km wide pinger array, as estimated from initial test deployments.

Moorings

To characterize the physical and hydrographic environment, an acoustic Doppler current profiler (ADCP) and thermistor chain (T-chain) were deployed within the pinger array in 20 m of water (Fig. 1). The bottom-mounted, upward-looking five-beam Teledyne RD Instruments Sentinel V ADCP sampled at 2 Hz with vertical bin sizes of 0.25 m. Adjacent to the ADCP was a taut mooring T-chain with 15 RBRsolo temperature sensors secured every meter along a line; at the top and bottom positions were Sea-Bird Scientific SBE-56 temperature sensors, while the middle position held an RBRduo temperature/pressure recorder. The ADCP and T-chain were deployed on the same isobath and were separated by 25 m in the cross-shore, and 105 m in the alongshore direction. The T-chain was configured to be taut relative to the bottom, and thus in the same frame of reference as the ADCP. Because the M-AUEs referenced their depth relative to the surface, which varies relative to the bottom as a function of the surface waves and tide, both the ADCP velocity records and the T-chain measurements were converted from distance above the bottom to depth below the surface. The velocity data were then linearly interpolated to a fixed-depth grid, with a vertical resolution of 0.25 m, and filtered in both the forward and backward direction, with a moving average window of 60 s in time, and 3 bins in depth. This filtering method was selected to avoid phase distortion of the signal. Temperature data for each T-chain logger were filtered using a 10-s moving average filter, and decimated to a common 10-s time vector before also being linearly interpolated to the same fixed-depth grid as the velocity data. Isotherm depth was estimated using linear interpolation between sensors. Because there was a small horizontal offset, the temperature and velocity time series of the moorings were aligned based on their respective internal wave arrival times.

Minute-averaged wind data were obtained from the Scripps Pier weather station, located 25 km to the north of the site, as measured with a RM Young 05106 anemometer and recorded using a Scripps DL4 Hydroclimate data logger.

Wave model

The Korteweg–de Vries (KdV) equation is one of the models commonly used to study shallow-water, weakly nonlinear internal waves (reviewed in Apel 2002). The better-known solitary wave solution to the KdV equation describes weakly nonlinear, nonsinusoidal internal waves. Cnoidal functions, cn, can be used to extend the KdV solutions to oscillatory waves with a broader range in nonlinearity (Apel 2002):

$$\eta(x,z,t) = \eta_c + \eta_{max}\phi(z)\mathrm{cn}^2(\gamma(x-ct);m) + d, \quad (1)$$

where η_c is the crest elevation (m), η_{max} is the maximum isopycnal displacement (m), $\phi(z)$ is the wave's vertical structure function, c is the wave propagation speed (m s^{-1}), t is time (s), m is the modulus of the Jacobi function cn, d is the mean value of η over a period, and

$$\gamma^2 = \frac{\alpha\eta_{max}}{12m\beta}. \quad (2)$$

In this case, x (m) is positive in the direction of wave propagation, and z (m) is positive up. Both the crest elevation and the wave propagation speed can be related to the complete elliptical integrals of the first and second kind, $K(m)$ and $E(m)$, respectively using
equation 1,

$$\eta_c = \frac{\eta_{max}}{m}\left(1 - m - \frac{E(m)}{K(m)}\right), \quad (3)$$

and

$$c = c_0 + d\alpha + \frac{\alpha\eta_{max}}{3}\left(\frac{2-m}{m} - 3\frac{E(m)}{mK(m)}\right). \quad (4)$$

equation 2.
Given this solution, the wavelength $\lambda = 2K(m)/\gamma$, with period $T = \lambda/c$.

As presented by Shroyer et al. (2009) and Grimshaw et al. (2004), the nonlinear and dispersive coefficients, α and β respectively, can be calculated from the linear wave propagation speed, c_0, and a background velocity profile, u_B, using

$$\alpha = \frac{3\int_{-H}^{0}(c_0-u_B)^2\left(\frac{\partial\phi(z)}{\partial z}\right)^3 dz}{2\int_{-H}^{0}(c_0-u_B)\left(\frac{\partial\phi(z)}{\partial z}\right)^2 dz}, \quad (5)$$

and

$$\beta = \frac{\int_{-H}^{0}(c_0-u_B)^2\phi^2 dz}{2\int_{-H}^{0}(c_0-u_B)\left(\frac{\partial\phi}{\partial z}\right)^2 dz}. \quad (6)$$

Here, ϕ and c_0 were calculated from our observed background stratification and velocities using Smyth et al.'s (2010) Taylor-Goldstein equation solver, following the method of Shroyer et al. (2011). Because the profiling Wirewalker showed that temperature dominated the vertical and temporal variability of density (not shown), we calculated the background stratification from temperature using a salinity of 33.5. The ADCP did not cover the top 3 m of the water column, so we varied the extrapolation of cross-shore velocities to the surface until the KdV flow field best matched the distribution and magnitude of cross-shore velocities measured at 3 m. We set d to zero, and used the computed values for c_0, α, and β, as well as our observed η_{max} and T to estimate m iteratively.

Wave-induced velocities are commonly defined as velocity anomalies relative to the unperturbed background velocity profile (e.g., Stastna and Lamb 2002), that is, they include contributions from the propagating wave and the deformation of the background velocities. We separate the wave- and background-velocity contributions to total velocities by using a tilde to denote the velocities associated with the deformed background profile ($\tilde{u}_B, \tilde{w}_B$) and reserve u_B for the un-deformed background profile ahead of the wave (Fig. 3). We calculate the wave velocities (u_W, w_W) by subtracting background velocities interpolated along isopycnals from total velocities (u_T, w_T) (Shroyer et al. 2010):

$$u_W = u_T - \tilde{u}_B, \tag{7}$$

and

$$w_W = w_T + \tilde{w}_B, \tag{8}$$

where $\tilde{u}_B(z) = u_B(z-\eta)$, and $\tilde{w}_B = 0$ due to negligible background vertical velocities.

Modeled organisms

To assess the effects of vertical swimming on horizontal transport, we introduced virtual organisms into the theoretical wave flow field. These organisms covered a range of swimming strategies, going from (1) Passive/Lagrangian, that is, they were advected by the wave and background horizontal and vertical velocities, to (2) Depth-keeping, that is, they exactly countered external vertical velocities, but were advected by horizontal velocities (*see* Scotti and Pineda 2007 for comments on depth-keeping vs. directed swimming).

Results

M-AUE transport

The M-AUE records revealed a 15- to 20-min time period with elevated temperatures that coincided with the M-AUEs' downward displacements and increased horizontal velocities

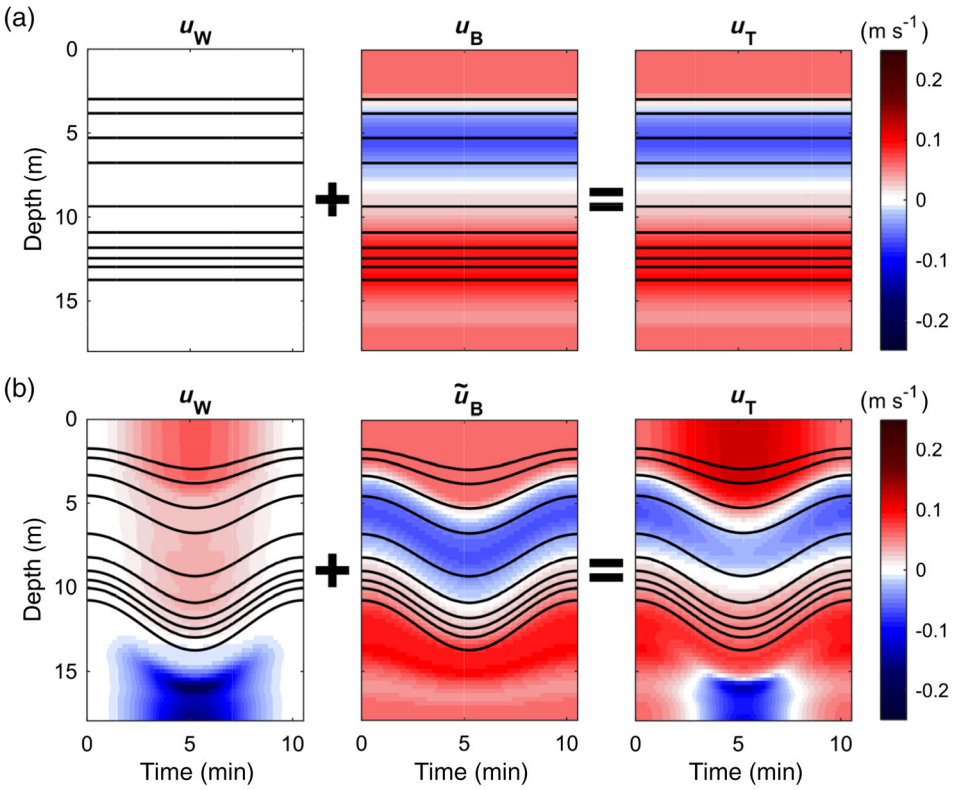

Fig. 3. Wave and background contributions to total cross-shore velocities, u_T (m s^{-1}). (**a**) Unperturbed background, u_B. (**b**) Wave event, with u_W showing the wave velocities and $\tilde{u}_B$ the deformed background velocities. Black lines show isopycnals and red is positive onshore.

onshore (Fig. 2). These data are consistent with an internal wave of depression propagating through the swarm, as the downward isotherm displacement will draw warm near-surface water past the depth-keeping M-AUEs. However, the M-AUEs were not perfectly depth-keeping, as can be seen by their ~ 1 m vertical excursions (Fig. 2e). Noting that the M-AUEs exhibited a time lag in their response to vertical displacement by the wave (Fig. 2e), and assuming that the wave's downward and upward vertical velocities were equal (as would be the case with a sinusoidal wave), the M-AUEs' maximum swimming speeds were estimated by subtracting their upward and downward velocities. Overall, the M-AUEs' vertical swimming velocities were < 0.15 cm s^{-1}.

As the wave trough passed, the seven M-AUEs were advected onshore, with net cross-shore displacements ranging from 30 to 70 m (mean of 50 m). None of the M-AUEs returned to their initial horizontal locations after the wave's passage (Fig. 2b,d), as would be expected in a linear internal wave without background currents. Because the Stokes drift in linear internal waves tends to be small compared to transport by strongly nonlinear waves (Lamb 1997), a reasonable hypothesis would be that a nonlinear internal wave moved the M-AUEs onshore. However, the maximum isotherm displacement during wave passage was small compared to the water depth (~ 10–15%), consistent with a linear or weakly nonlinear wave. These observations suggested that some other mechanism contributed to the observed cross-shore transports.

Background velocities

A spectral analysis of our ADCP time series of cross-shore velocities showed that variance was elevated in both the near-*f* and M2 tidal frequencies (Fig. 4). A band-pass filter centered between 1/14.5 and 1/11 cycles h^{-1} was used to isolate the M2 velocities (Lerczak 2000). Over the 14-d period, depth-independent (barotropic) cross-shore tidal velocities reached a maximum of 0.03 m s^{-1}, while the amplitude of the mode-1 baroclinic (internal) tide reached a maximum of 0.08 m s^{-1} (Fig. 5e). Although the barotropic tidal velocity was onshore during the M-AUE deployment, baroclinic velocities in the upper half of the water column were negative (offshore), and background cross-shore velocities at 3-m depth were only 0.02 m s^{-1} (Fig. 5c). Background velocities alone can, therefore, account for only about half of the ~ 50-m mean M-AUE cross-shore transport (Table 1). The observed background velocity profile was within the variability of hourly averaged currents measured throughout the 14-d deployment (Figs. 5c, 6).

Wave event

Nearly 50 min after propagating through the M-AUE swarm, the internal wave event was recorded at both the ADCP and T-chain (Fig. 5b, Wave). Based on these arrival times and the 10.5-min wave period, *T*, measured at the ADCP, the wave's cross-shore propagation speed, *c*, and its

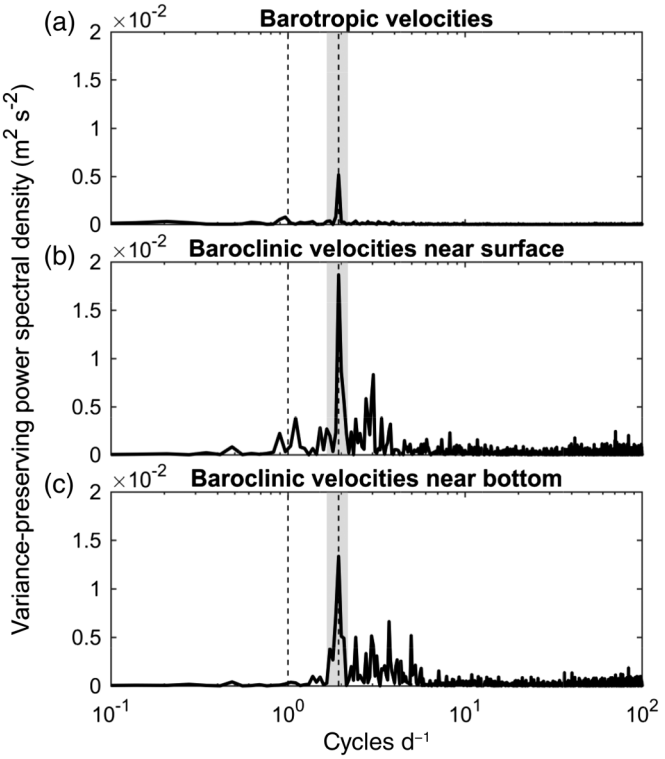

Fig. 4. Variance-preserving power spectral density (m^2 s^{-2}) of total cross-shore (**a**) barotropic velocities, (**b**) baroclinic velocities near the surface (z = −4 m), and (**c**) baroclinic velocities near the bottom (z = −18 m). The dashed lines show the diurnal and M2 frequencies, with the frequency band used to isolate the M2 tide (Fig. 5e) in gray.

cross-shore wavelength, λ, were estimated to be 0.3 m s^{-1} and 190 m, respectively. At the T-chain, the wave had a maximum isotherm displacement of ~ 3 m. Although an internal wave appears to have preceded the wave of interest (Fig. 5b), we focus on the second wave because of its stronger and more complete signal in the M-AUE record.

Prior to the wave's arrival, background cross-shore velocities were negative/offshore approximately between 3- and 8-m depth, and positive/onshore below (Fig. 5b, Background). Background cross-shore velocities above 3-m depth appeared to be positive/onshore, possibly due to the afternoon sea breeze blowing onshore (Fig. 5a). As it propagated past the ADCP and T-chain, the internal wave appears to have vertically deformed this along-isopycnal, surface-intensified, onshore background flow downward, drawing positive/onshore velocities downward to depths as great as 6 m (Fig. 5b, Wave). The total transport experienced by the M-AUEs was, therefore, a combination of both the wave's velocities and the deformed background velocities.

KdV model

To address the lack of ADCP coverage in the top 3 m, various extrapolations of cross-shore background velocities toward the surface were tested to find the best match of the

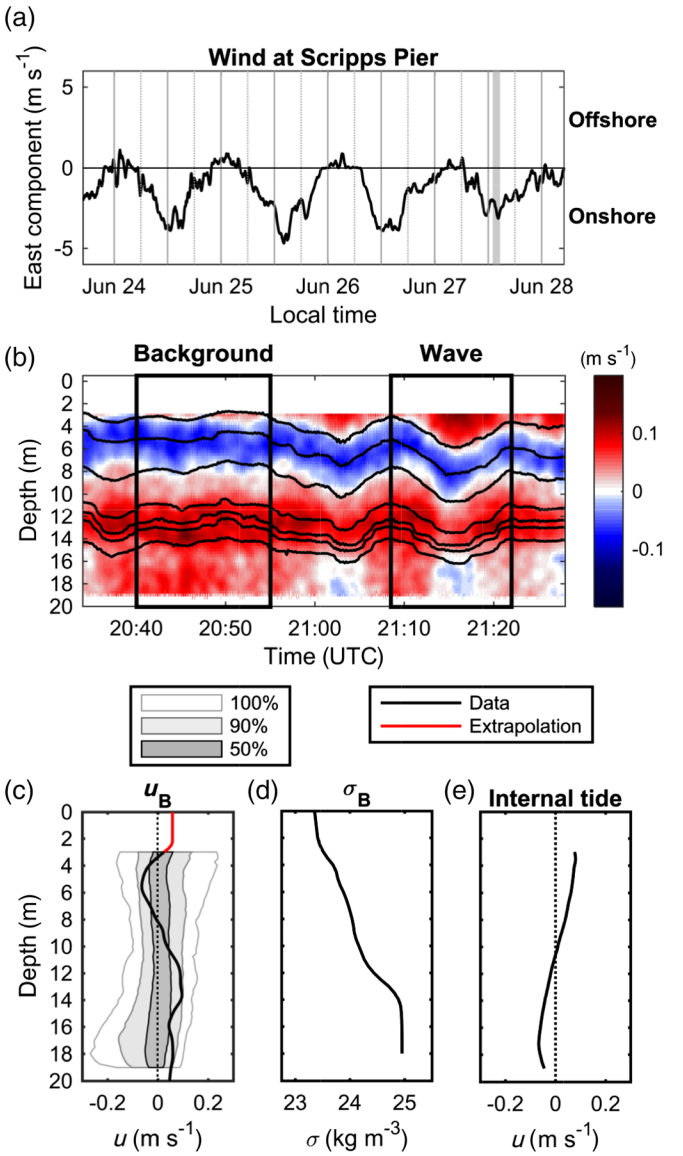

Fig. 5. Wave and background flow properties. (**a**) Thirty-minute moving average of east component of the wind (m s^{-1}) measured at the Scripps Pier. Negative values indicate wind blowing from the west (i.e., onshore). The M-AUE deployment time is shown by the gray box. (**b**) ADCP time series. The black rectangles show the wave of interest (right box), as well as the time period over which the mean background velocity and stratification profiles were calculated (left box). (**c**) Mean cross-shore background velocities (m s^{-1}), calculated every 0.25 m (black line), and extrapolation of background velocities to the surface, as described for the KdV 2 model (red line) (Fig. 7). The shaded areas show the envelopes containing 100%, 90%, and 50% of the low-pass filtered velocity data (< 1 cycle h^{-1}) shown in Fig. 6. The dotted line shows zero cross-shore velocity. (**d**) Background density profile (kg m^{-3}). (**e**) Maximum cross-shore velocity amplitude of the M2 baroclinic tide. This vertical structure explains 85% of the M2 baroclinic variance. The dotted line shows zero cross-shore velocity.

KdV model to observations. A constant extrapolation of background velocities measured at 3-m depth to the surface produced a wave of elevation from the KdV model (Fig. 7, KdV 1),

Table 1. Total cross-shore transport experienced by depth-keepers at 3 m depth, over a wave period. Values are positive onshore.

Source of estimate	Δx (m)	τ (min)
M-AUEs (n = 7)	30–70	15–20
KdV simulation		
Full simulation, $u_W + \tilde{u}_B$	95	17
Using wave velocities alone, u_W	25	12
Using background velocities alone*, u_B	25	17*
ADCP		
Integrated	55	10.5
Propagated with c = 0.3 m s^{-1}	90	15

*Time of integration determined by residence time in the full wave.

while observations indicate that a wave of depression propagated through the M-AUEs. Experiments showed that positive, surface-intensified velocities above 3 m were necessary to reverse the polarity predicted by the model from a wave of elevation to a wave of depression such as was observed (e.g., Fig. 7, KdV 2). Testing a range of cases, it became clear that an extrapolation of the vertical shear to 2.5 m, with velocities then held constant to the surface (Fig. 5c) best reproduced the distribution and magnitude of cross-shore velocities measured at the ADCP (Fig. 8). The observed wave period was best reproduced when m = 0.13; however, the calculated η_c had to be set to zero for isopycnals to return to their unperturbed depths at the internal wave crests, as observed (Fig. 5b). It is unclear whether isopycnals did indeed return to their unperturbed depths, or if this impression was a result of the background being calculated at a time when isopycnals were raised, despite appearing flat. Nevertheless, the flow field associated with the modeled wave of depression in Fig. 7 (KdV 2) was an excellent match to observations, and subsequent references to a theoretical/KdV flow field will imply this specific solution. The 0.23 m s^{-1} wave propagation speed associated with the KdV solution selected was 25% less than the field estimate based on the wave arrival times at the M-AUEs and mooring; however, it is not uncommon for theory to underestimate wave propagation speeds (Lien et al. 2012). The calculated value of m was small, supporting the hypothesis that the observed wave was only weakly nonlinear.

Transport of modeled organisms

To estimate total cross-shore transport of organisms in the wave, virtual organisms with swimming behaviors ranging from completely passive to depth-keeping were seeded at 3 m depth in the theoretical flow fields generated from the KdV equation (Fig. 7, KdV 2). The total cross-shore transport

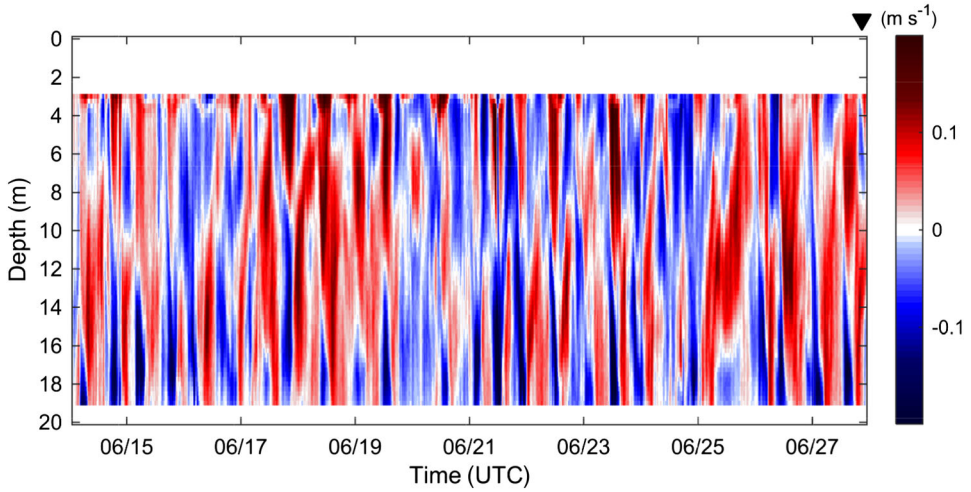

Fig. 6. Low-pass filtered (< 1 cycle h^{-1}) cross-shore velocities (m s^{-1}) measured at the ADCP during the full 14-d deployment. The black triangle shows the time of the M-AUE deployment. Positive velocities are onshore.

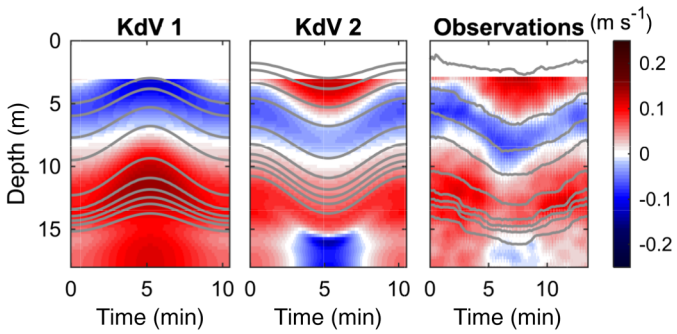

Fig. 7. Observation and model comparisons. The background velocity profile in KdV 1 has the velocity measured at 3-m depth held constant to the surface, while in KdV 2 the background vertical shear measured at 3 m is extrapolated to 2.5-m depth, with velocity then held constant to the surface. Red colors are positive onshore and in the direction of the wave propagation. The gray lines show isopycnals every 0.15 kg m^{-3}.

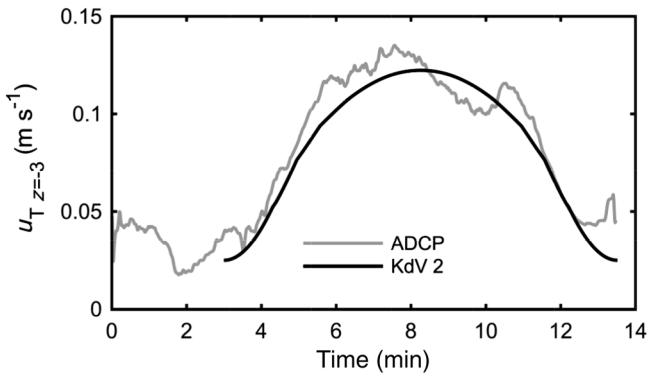

Fig. 8. Total cross-shore velocity (m s^{-1}) at 3-m depth. The gray line shows 30-s smoothed ADCP measurements, while the black line shows the KdV 2 velocities (Fig. 7).

distance experienced by modeled depth-keeping organisms was ~ 95 m, with a residence time in the wave, τ, of ~ 17 min (Fig. 9). Propagating virtual depth-keepers in the velocities captured by the ADCP during the wave event yielded a transport estimate of ~ 90 m with residence time of ~ 15 min, showing good agreement with the theoretical estimate.

Horizontal transport of modeled passive organisms in the same wave flow field and depth was estimated to be ~ 50 m, with a residence time of ~ 14 min. Transport distances and residence times for weak swimmers fell somewhere between those associated with passive and depth-keeping organisms (Fig. 9). In comparison, the total cross-shore transport of the M-AUEs ranged approximately from 30 to 70 m (mean 50 m), with residence times from 15 to 20 min. Seeding passive and depth-keeping organisms throughout the water column of the KdV flow field yielded residence time estimates ranging from 9 to 17 min, with cross-shore transport ranging from roughly –25 to 95 m onshore (Fig. 10).

Discussion

A drifting swarm of M-AUE larval mimics programmed to maintain 3-m depth was observed to suddenly move onshore, with net horizontal displacements of 30–70 m over 15–20 min. The anomalously warm waters recorded by the M-AUEs were consistent with them being transported in the trough of an internal wave. However, the amplitude of the internal wave indicated that it was not a highly nonlinear wave. Data analysis and modeling support the hypothesis that the M-AUEs were advected onshore in a combination of wave-generated currents, and wave-deformed background currents: a weakly nonlinear internal wave brought surface-intensified onshore currents down to the depths of the M-AUEs, boosting them onshore. This mechanism not only led to enhanced

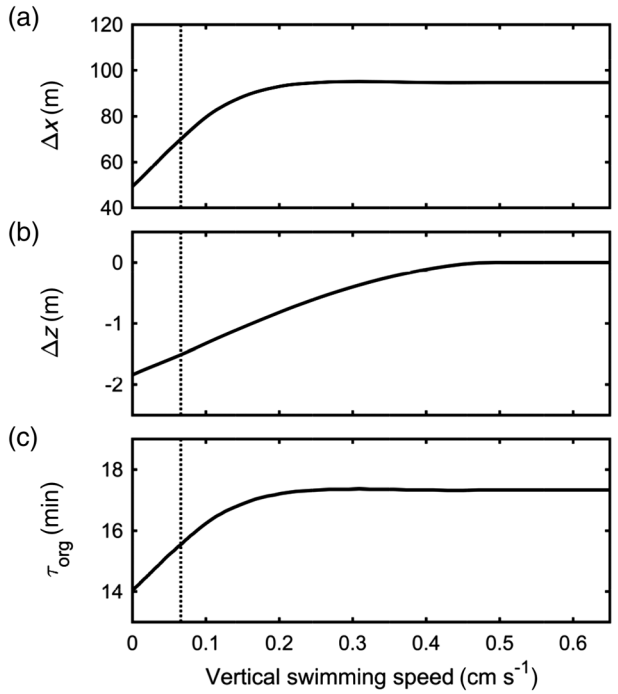

Fig. 9. (**a**) Total cross-shore transport (m), (**b**) maximum vertical displacement (m), and (**c**) residence time of organisms in the KdV 2 theoretical flow field (Fig. 7), as a function of swimming speed (cm s^{-1}). The dotted line shows the predicted vertical swimming speed associated with the maximum cross-shore transport experienced by the M-AUEs (70 m).

onshore velocities of the M-AUEs, it also extended the time the M-AUEs spent in the wave, further enhancing their onshore transport.

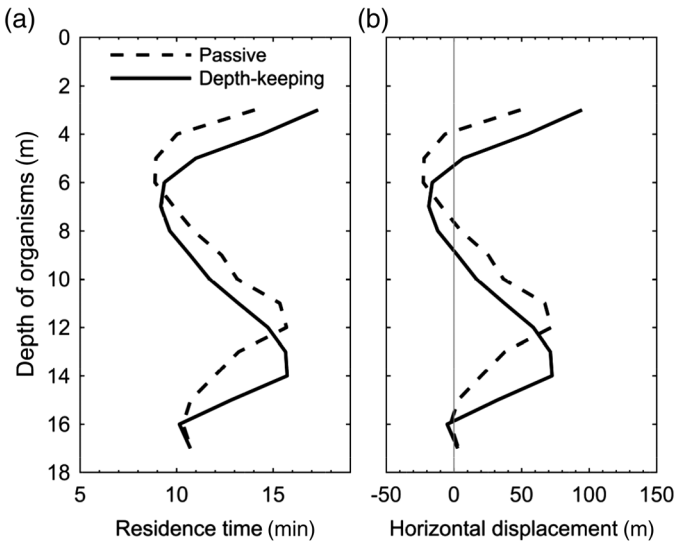

Fig. 10. (**a**) Residence time (min) and (**b**) total cross-shore displacement (m) experienced by passive/Lagrangian (dashed) and depth-keeping organisms (solid) in the KdV 2 theoretical flow field (Fig. 7). Depth is based on vertical position at the crest of the waves. The thin gray line in (**b**) shows zero net transport.

Mechanisms of transport

As the wave of depression propagated through the M-AUEs and past the moorings, the downward deflection of the isotherms also drew the surface-intensified, along-isopycnal background horizontal velocities downward (Fig. 11). Above 6 m, background cross-shore velocities at any given depth were increased by this downward deformation of the fast-moving near-surface currents (Fig. 5b, Wave). The M-AUEs and any organisms that could maintain depth in the wave's trough thus experienced total cross-shore velocities that were a combination of the wave's velocities at that depth, and the higher background velocities, $\tilde{u}_B$, drawn downward by the wave from shallower depths. Passive organisms, on the other hand, would have felt only the wave velocities embedded in a steady background velocity. Thus, in this vertically sheared, wave-perturbed flow field, any depth-keeping behavior would have exposed organisms to nonsteady, onshore, background velocities and resulted in increased cross-shore transport (Fig. 11).

The largest transports experienced by the M-AUEs were within the range expected for plankton with vertical swimming speeds of ~ 0.05–0.1 cm s^{-1} (Fig. 9a). Swimming speeds on the order of 0.1–1 cm s^{-1} are well within the abilities of many larvae (Mileikovsky 1973; Chia et al. 1984; Weidberg et al. 2014), and zooplankton such as the Antarctic krill (Murphy et al. 2013). With vertical swimming speeds < 0.15 cm s^{-1}, the M-AUEs are thus representative of fairly weak swimmers; stronger swimmers would have experienced even larger cross-shore transports in the observed wave. Although the maximum vertical velocities associated with the wave were ~ 1–2 cm s^{-1}, our results show that swimming speeds of ~ 0.25 cm s^{-1} would have been sufficient to experience the same onshore transport as the strongest depth-keepers (Fig. 9a).

The total cross-shore transport of any organism over a wave period, Δx_{org}, can be calculated by summing the wave's cross-shore velocities and any additional contribution to cross-shore velocities experienced over time (Lamb 1997). In our case, we assumed no horizontal swimming, so additional contributions are limited to the background current:

$$\Delta x_{org} = \int_{t1}^{t2} \left[u_W\left(x_{org}, z_{org}, t\right) + \tilde{u}_B\left(x_{org}, z_{org}, t\right) \right] dt, \qquad (9)$$

where x_{org} and z_{org} represent the horizontal and vertical position of the organism, respectively, and $t1$ and $t2$ are times immediately as the organism enters and exits the wave, respectively. Importantly, because of the wave's deformation of the vertically sheared background current, the $\tilde{u}_B$ experienced by even weakly depth-keeping organisms will vary significantly over the wave's cycle.

An important result arising from Eq. 9 is that the total transport of planktonic organisms cannot be estimated by summing the total transport due to the wave and to

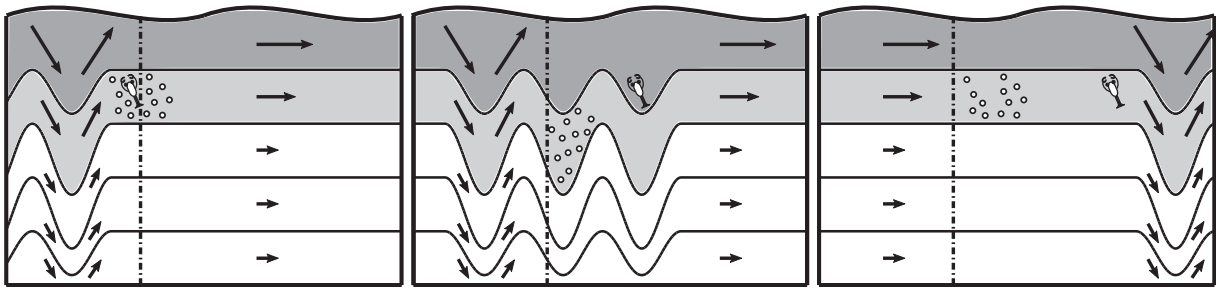

Fig. 11. Schematic of plankton transport induced by internal-wave deformation of a surface-intensified, vertically sheared background current (black arrows and shading). As the internal wave train propagates to the right, it deforms along-isopycnal background velocities. Passive phytoplankton (circles) are moved up and down by the waves and experience constant background velocities, while depth-keeping zooplankton (lobster larvae) are exposed to higher background velocities. Overall, depth-keeping plankton experience greater onshore transport than passive plankton due to both increased velocities and increased residence time in the waves. The black dash-dot line shows the organisms' initial horizontal positions.

background currents independently (e.g., Table 1). Rather, Eq. 9 shows that because the background current influences the position of an organism with respect to the wave, both wave and background velocities must be integrated simultaneously along the organism's path over time. Obtaining subsurface, time-varying, three-dimensional trajectories in the ocean at spatial and temporal scales relevant to high-frequency internal waves is technologically challenging. Using mooring (i.e., Eulerian) velocities to predict transport, however, must be done with caution. Equation 9 relies on the velocities as experienced by the organisms; substituting a time series of measured mooring velocities for u_W and $\tilde{u}_B$ will not account for how organisms experience the flow, that is, their residence time in various parts of the wave.

The important difference between Eulerian and Lagrangian frames of reference can be illustrated using time series from the virtual depth-keeping organisms seeded in the KdV theoretical flow field (Fig. 12). Though the results are specific to this simulation, the principles apply to any wave field. Integrating the total velocities as sampled by a virtual mooring at 3-m depth over a wave period (Fig. 12c, solid line) predicts an onshore transport of ~ 40 m, in contrast to the ~ 95 m transport obtained for depth-keeping organisms seeded at the same depth in the same flow. Comparing the velocity time series obtained from the mooring (Fig. 12c, solid line) and the velocity time series of an advected organism (Fig. 12b, solid line) shows the difference between the two measurements: organisms traveling with the wave spent more time in the wave's trough where the directions of the wave and background velocities aligned.

Stokes drift is derived from the difference between predictions of travel paths and Eulerian measurements over a wave period. It is important to note, however, that the duration of a "wave period" experienced by an organism is distinct from the wave period itself, and also depends on background currents. For instance, in our simulation, background currents increased the residence time of depth-keepers in the wave to ~ 17 min (Fig. 3b, solid line, Table 1), compared with a ~ 12-min residence time associated with the wave velocities alone (Fig. 3b, dashed line, Table 1). This phenomenon arises from Doppler shifting of the wave in a moving reference frame (the background current). We note that the comparisons between results derived from the full flow field vs. the wave velocities alone are for illustrative purposes and neglect the fact that without background currents, the wave shape would be different.

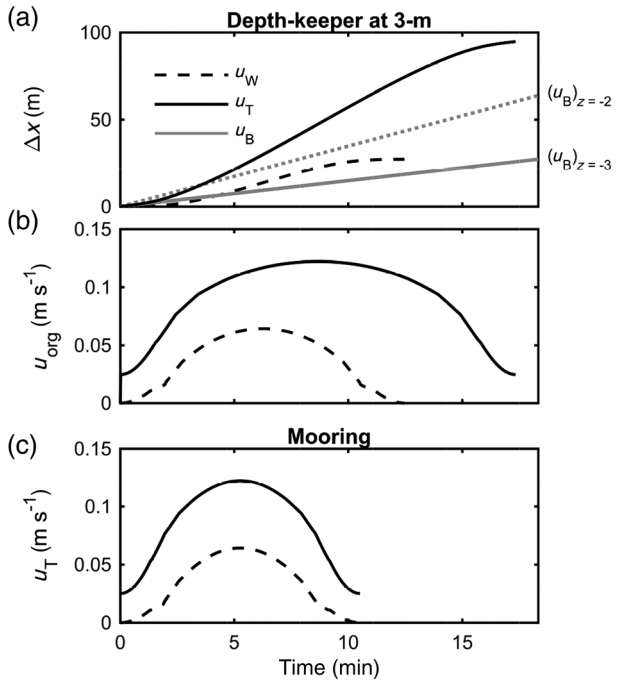

Fig. 12. Cross-shore transport and velocity of depth-keepers and at a simulated mooring over a wave period, using the KdV 2 theoretical flow field (Fig. 7). (**a**) Cross-shore displacement of 3-m depth-keepers associated with wave velocities alone (black dashed line), and with total velocities over a wave period (black solid line). Gray lines show the displacement associated with the unperturbed background current alone, at 2 m (dotted) and 3 m (solid) depth. (**b**) Cross-shore velocity of 3-m depth-keepers when propagated using wave velocities alone (dashed line) and using total velocities (solid line), over a wave period. Positive velocities are onshore and negative velocities are offshore. (**c**) Cross-shore velocity at 3 m depth, as sampled by a mooring. Wave velocities are in dashed, and total velocities are in solid.

In general, any background current will affect the transport of both depth-keeping and passive plankton by modulating the total velocities these organisms experience. These background-influenced velocities will in turn influence the time the organisms spend in the wave. When wave propagation speed estimates can be obtained, numerically propagating virtual organisms in a wave-perturbed flow measured by an ADCP will yield better larval transport estimates than simply integrating ADCP velocities (Table 1). Including horizontal swimming of 1–5 cm s^{-1} in realistic numerical simulations of the central California upwelling system has been shown to increase larval supply to the nearshore (Drake et al. 2018); although neglected here, horizontal swimming in the direction of wave propagation could also enhance an organism's residence time in the wave and thus total transport (Shanks 1995). However, we have shown that a wave-deformed, vertically sheared background current obviates the need to invoke any directed horizontal swimming by the plankton.

Vertical structure of velocities

Overall, transport estimates are sensitive to the magnitude, direction, and vertical structure of the background current, the period and direction of the wave, as well as plankton horizontal and vertical swimming behavior (Lamb 1997; Franks et al. In press). For waves of depression, enhanced onshore transport will occur when the background currents above swimming organisms are in the onshore direction, as they were with the M-AUEs in this study. This can be seen from the virtual organisms seeded throughout the water column in our theoretical flow field (Fig. 10). Because of the depth-dependence of both background and wave cross-shore velocities, the total transport experienced by both depth-keeping and passive organisms was strongly dependent on their release depth (Fig. 10). The background current yielded greatest horizontal transport for depth-keeping organisms at some depths, and for passive organisms at other depths. In comparison, wave velocities alone would generate weaker transports throughout the model water column for both depth-keeping and passive organisms (Franks et al. In press).

An earlier study slightly north of our field site documented cross-shore variation in concentrations of barnacle nauplii and cyprids: the concentrations of the nauplii increased with distance from shore, while the concentrations of the cyprids, which are stronger swimmers, were higher closer to shore (Hagerty et al. 2018). This pattern was consistent with other studies (Tapia and Pineda 2007; Weidberg et al. 2014), and was more pronounced in spring–summer when stratification would support internal waves. Our observations suggest a possible mechanism driving these differing distributions: passive nauplii may experience weak onshore/offshore transport due to internal waves, while near surface depth-keeping cyprids are brought onshore by the combination of internal waves and deformed, surface-intensified background currents. Likewise, the variability in transport of surface drifters reported by Shanks (1983), which was attributed to linear vs. nonlinear internal waves (Shanks 1995; Pineda 1999), may also have arisen from a wave-current interaction similar to that described here.

The vertical structure of background velocities will be determined by a variety of dynamics on timescales longer than the high-frequency internal waves, including the sea breeze, the internal tide, and other lower-frequency flows. In regions where the sea breeze drives a strong onshore surface flow, such as the coast of California (Hendrickson and MacMahan 2009), the phasing of the sea breeze, the internal tide, and high-frequency internal wave activity will vary from day to day, leading to variations in larval transport (Hill 1998). Tapia and Pineda (2007), for instance, reported higher cyprid settlement after a day of sustained onshore winds. Alternately, where background velocities are predominantly driven by the internal tide, nonlinear wave trains may be phase-locked with preferentially onshore surface currents, as observed in the South China Sea (Alford et al. 2010). Prior studies at our site found cross-shore velocities on the shelf to be predominantly driven by a near-inertial response to the diurnal sea breeze and semidiurnal baroclinic tidal motions (Lerczak 2000; Lucas et al. 2011*b*). Spectral analysis of our ADCP time series confirmed elevated cross-shore variability at both the near-*f* and M2 tidal frequencies, but the direct effects of the sea breeze could not be distinguished from higher tidal modes due to a lack of velocity data in the top 3 m.

Although this study focused on the transport implications of internal waves deforming background velocities specific to depth-keeping plankton, it is worth noting that the vertical structure of background velocities will also affect the shape and period of the internal waves planktonic organisms will experience (Fig. 7), and thus their transport.

Conclusions

A deployment of seven subsurface vehicles, the M-AUEs, programmed to mimic planktonic depth-keeping behavior showed a pronounced onshore transport during the passage of an internal wave. In situ data and results from simple models showed that depth-keeping organisms can experience increased cross-shore transport through an internal wave-mediated deformation of a vertically sheared background current. By displacing isopycnals and high-velocity surface waters downward, internal wave troughs can increase both the residence time and total transport of organisms capable of even weak depth-keeping behavior. A KdV model, parameterized with mooring data, reproduced transport of the M-AUEs remarkably well: both model and observations showed that onshore transport on the order of 100 m could take place over 15–20 min, as internal waves displaced faster background cross-shore surface velocities downward to the M-AUE depths. The increased cross-shore transport associated with the time-varying background velocities experienced by organisms

capable of vertical swimming is mathematically analogous to the increase in onshore transport associated with horizontal swimming in highly nonlinear internal waves (Shanks 1995; Lamb 1997): "residence time" in the wave is increased relative to a case without swimming or vertically sheared background velocities. However, to experience a similar enhancement in transport, exploiting the deformation of a strongly sheared background flow requires much weaker swimming speeds than swimming horizontally, and is thus energetically less costly to organisms.

Predictions of larval transport will be improved by quasi-Lagrangian measurements of high-frequency physical processes and better understanding of plankton swimming behaviors (Metaxas and Saunders 2009). Given the predictability of the diurnal sea breeze in many areas, including the coast of Southern California (Dorman 1982; Lerczak et al. 2003), it is conceivable that populations of some organisms have adapted to exploit the interacting wind and internal wave velocity fields to enhance their onshore transport. Other mechanisms could also drive a vertically sheared background current in other areas; larvae located near riverine input, for instance, could maintain depth at optimum salinity concentrations and benefit from internal waves propagating offshore for dispersal (Nash and Moum 2005). Ultimately, the direction of the transport boosts will be set by the shallower background currents advected by internal waves to the depths of the depth-keeping organisms.

References

Alford, M. H., R.-C. Lien, H. Simmons, J. M. Klymak, S. Ramp, Y.-J. Yang, D. Tang, and M.-H. Chang. 2010. Speed and evolution of nonlinear internal waves transiting the South China Sea. J. Phys. Oceanogr. **40**: 1338–1355. doi:10.1175/2010JPO4388.1

Apel, J. R. 2002. Oceanic internal waves and solitons, p. 1–40. *In* C. R. Jackson and J. R. Apel [eds.], An atlas of internal solitary-like waves and their properties. Global Ocean Associates.

Apel, J. R., J. R. Holbrook, A. K. Liu, and J. J. Tsai. 1985. The Sulu Sea internal soliton experiment. J. Phys. Oceanogr. **15**: 1625–1651. doi:10.1175/1520-0485(1985)015<1625:TSSISE>2.0.CO;2

Armstrong, F. A. J., and E. C. LaFond. 1966. Chemical nutrient concentrations and their relationship to internal waves and turbidity off Southern California. Limnol. Oceanogr. **11**: 538–547. doi:10.4319/lo.1966.11.4.0538

Chia, F.-S., J. Buckland-Nicks, and C. M. Young. 1984. Locomotion of marine invertebrate larvae: A review. Can. J. Zool. **62**: 1205–1222. doi:10.1139/z84-176

Cleveland, W. S., and E. Grosse. 1991. Computational methods for local regression. Stat. Comput. **1**: 47–62. doi:10.1007/BF01890836

Colosi, J. A., N. Kumar, S. H. Suanda, T. M. Freismuth, and J. MacMahan. 2018. Statistics of internal tide bores and internal solitary waves observed on the inner continental shelf off Point Sal, California. J. Phys. Oceanogr. **48**: 123–143. doi:10.1175/JPO-D-17-0045.1

Cragg, S. M. 1980. Swimming behaviour of the larvae of *Pecten maximus* (L.) (Bivalvia). J. Mar. Biol. Assoc. U. K. **60**: 551–564. doi:10.1017/S002531540004025X

Daigle, R. M., and A. Metaxas. 2011. Vertical distribution of marine invertebrate larvae in response to thermal stratification in the laboratory. J. Exp. Mar. Biol. Ecol. **409**: 89–98. doi:10.1016/j.jembe.2011.08.008

Dewar, W. K. 1980. The effect of internal waves on neutrally buoyant floats and other near-Lagrangian tracers. M.S. thesis. Massachusetts Institute of Technology.

DiBacco, C., H. L. Fuchs, J. Pineda, and K. Helfrich. 2011. Swimming behavior and velocities of barnacle cyprids in a downwelling flume. Mar. Ecol. Prog. Ser. **433**: 131–148. doi:10.3354/meps09186

Dorman, C. E. 1982. Winds between San Diego and San Clemente Island. J. Geophys. Res. **87**: 9636–9646. doi:10.1029/JC087iC12p09636

Drake, P. T., C. A. Edwards, S. G. Morgan, and E. V. Satterthwaite. 2018. Shoreward swimming boosts modeled nearshore larval supply and pelagic connectivity in a coastal upwelling region. J. Mar. Syst. **187**: 96–110. doi:10.1016/j.jmarsys.2018.07.004

Franks, P. J. S. 1997. Spatial patterns in dense algal blooms. Limnol. Oceanogr. **42**: 1297–1305. doi:10.4319/lo.1997.42.5_part_2.1297

Franks, P. J. S., J. C. Garwood, M. Ouimet, J. Cortes, R. C. Musgrave, and A. J. Lucas. In press. Stokes drift of plankton in linear internal waves: Cross-shore transport of neutrally buoyant and depth-keeping organisms. Limnol. Oceanogr. doi:10.1002/lno.11389

Fuchs, H. L., L. S. Mullineaux, and A. R. Solow. 2004. Sinking behavior of gastropod larvae (*Ilyanassa obsoleta*) in turbulence. Limnol. Oceanogr. **49**: 1937–1948. doi:10.4319/lo.2004.49.6.1937

Fuchs, H. L., E. J. Hunter, E. L. Schmitt, and R. A. Guazzo. 2013. Active downward propulsion by oyster larvae in turbulence. J. Exp. Biol. **216**: 1458–1469. doi:10.1242/jeb.079855

Fujimura, A. G., A. J. H. M. Reniers, C. B. Paris, A. L. Shanks, J. H. Macmahan, and S. G. Morgan. 2014. Numerical simulations of larval transport into a rip-channeled surf zone. Limnol. Oceanogr. **59**: 1434–1447. doi:10.4319/lo.2014.59.4.1434

Genin, A., J. S. Jaffe, R. Reef, and C. Richter. 2005. Swimming against the flow: A mechanism of zooplankton aggregation. Science **308**: 860–862. doi:10.1126/science.1107834

Grimshaw, R., E. Pelinovsky, T. Talipova, and A. Kurkin. 2004. Simulation of the transformation of internal solitary waves on oceanic shelves. J. Phys. Oceanogr. **34**: 2774–2791. doi:10.1175/JPO2652.1

Hagerty, M. L., N. Reyns, and J. Pineda. 2018. Constrained nearshore larval distributions and thermal stratification. Mar. Ecol. Prog. Ser. **595**: 105–122. doi:10.3354/meps12561

Helfrich, K. R., and J. Pineda. 2003. Accumulation of particles in propagating fronts. Limnol. Oceanogr. **48**: 1509–1520. doi:10.4319/lo.2003.48.4.1509

Hendrickson, J., and J. MacMahan. 2009. Diurnal Sea breeze effects on inner-shelf cross-shore exchange. Cont. Shelf Res. **29**: 2195–2206. doi:10.1016/j.csr.2009.08.011

Hill, A. E. 1998. Diel vertical migration in stratified tidal flows: Implications for plankton dispersal. J. Mar. Res. **56**: 1069–1096. doi:10.1357/002224098765173464

Inall, M. E., G. I. Shapiro, and T. J. Sherwin. 2001. Mass transport by non-linear internal waves on the Malin Shelf. Cont. Shelf Res. **21**: 1449–1472. doi:10.1016/S0278-4343(01)00020-6

Jaffe, J. S., P. J. S. Franks, P. L. D. Roberts, D. Mirza, C. Schurgers, R. Kastner, and A. Boch. 2017. A swarm of autonomous miniature underwater robot drifters for exploring submesoscale ocean dynamics. Nat. Commun. **8**: 1–8. doi:10.1038/ncomms14189

Klymak, J. M., R. Pinkel, C. Liu, A. K. Liu, and L. David. 2006. Prototypical solitons in the South China Sea. Geophys. Res. Lett. **33**: L11607. doi:10.1029/2006GL025932

Lamb, K. G. 1997. Particle transport by nonbreaking, solitary internal waves. J. Geophys. Res. **102**: 18641–18660. doi:10.1029/97JC00441

Largier, J. L. 2003. Considerations in estimating larval dispersal distances from oceanographic data. Ecol. Appl. **13**: 71–89. doi:10.1890/1051-0761(2003)013[0071:CIELDD]2.0.CO;2

Lennert-Cody, C. E., and P. J. S. Franks. 1999. Plankton patchiness in high-frequency internal waves. Mar. Ecol. Prog. Ser. **186**: 59–66. doi:10.3354/meps186059

Lennert-Cody, C. E., and P. J. S. Franks. 2002. Fluorescence patches in high-frequency internal waves. Mar. Ecol. Prog. Ser. **235**: 29–42. doi:10.3354/meps235029

Lerczak, J. A. 2000. Internal waves on the Southern California Shelf. PhD Dissertation. Univ. of California, San Diego.

Lerczak, J. A., C. D. Winant, and M. C. Hendershott. 2003. Observations of the semidiurnal internal tide on the southern California slope and shelf. J. Geophys. Res. Oceans **108**: 3068. doi:10.1029/2001JC001128

Lien, R.-C., E. A. D'Asaro, F. Henyey, M.-H. Chang, T.-Y. Tang, and Y.-J. Yang. 2012. Trapped core formation within a shoaling nonlinear internal wave. J. Phys. Oceanogr. **42**: 511–525. doi:10.1175/2011JPO4578.1

Lucas, A. J., C. L. Dupont, V. Tai, J. L. Largier, B. Palenik, and P. J. S. Franks. 2011*a*. The green ribbon: Multiscale physical control of phytoplankton productivity and community structure over a narrow continental shelf. Limnol. Oceanogr. **56**: 611–626. doi:10.4319/lo.2011.56.2.0611

Lucas, A. J., P. J. S. Franks, and C. L. Dupont. 2011*b*. Horizontal internal-tide fluxes support elevated phytoplankton productivity over the inner continental shelf. Limnol. Oceanogr.: Fluids Environ. **1**: 56–74. doi:10.1215/21573698-1258185

Metaxas, A., and M. Saunders. 2009. Quantifying the "bio-" components in biophysical models of larval transport in marine benthic invertebrates: Advances and pitfalls. Biol. Bull. **216**: 257–272. doi:10.2307/25548159

Mileikovsky, S. A. 1973. Speed of active movement of pelagic larvae of marine bottom invertebrates and their ability to regulate their vertical position. Mar. Biol. **23**: 11–17. doi:10.1007/BF00394107

Morgan, S. G., J. L. Fisher, S. H. Miller, S. T. Mcafee, and J. L. Largier. 2009. Nearshore larval retention in a region of strong upwelling and recruitment limitation. Ecology **90**: 3489–3502. doi:10.1890/08-1550.1

Morgan, S. G., A. L. Shanks, J. Macmahan, A. J. H. M. Reniers, C. D. Griesemer, M. Jarvis, and A. G. Fujimura. 2017. Surf zones regulate larval supply and zooplankton subsidies to nearshore communities. Limnol. Oceanogr. **62**: 2811–2828. doi:10.1002/lno.10609

Murphy, D. W., D. R. Webster, and J. Yen. 2013. The hydrodynamics of hovering in Antarctic krill. Limnol. Oceanogr.: Fluids Environ. **3**: 240–255. doi:10.1215/21573689-2401713

Nash, J., E. Shroyer, S. Kelly, and M. Inall. 2012. Are any coastal internal tides predictable? Oceanography **25**: 80–95. doi:10.5670/oceanog.2012.44

Nash, J. D., and J. N. Moum. 2005. River plumes as a source of large-amplitude internal waves in the coastal ocean. Nature **437**: 400–403. doi:10.1038/nature03936

Omand, M. M., J. J. Leichter, P. J. S. Franks, R. T. Guza, A. J. Lucas, and F. Feddersen. 2011. Physical and biological processes underlying the sudden surface appearance of a red tide in the nearshore. Limnol. Oceanogr. **56**: 787–801. doi:10.4319/lo.2011.56.3.0787

Peterson, W. T., C. B. Miller, and A. Hutchinson. 1979. Zonation and maintenance of copepod populations in the Oregon upwelling zone. Deep-Sea Res. Part A Oceanogr. Res. Pap. **26**: 467–494. doi:10.1016/0198-0149(79)90091-8

Pineda, J. 1999. Circulation and larval distribution in internal tidal bore warm fronts. Limnol. Oceanogr. **44**: 1400–1414. doi:10.4319/lo.1999.44.6.1400

Pinkel, R., M. A. Goldin, J. A. Smith, O. M. Sun, A. A. Aja, M. N. Bui, and T. Hughen. 2011. The Wirewalker: A vertically profiling instrument carrier powered by ocean waves. J. Atmos. Ocean. Technol. **28**: 426–435. doi:10.1175/2010JTECHO805.1

Rainville, L., and R. Pinkel. 2001. Wirewalker: An autonomous wave-powered vertical profiler. J. Atmos. Ocean. Technol. **18**: 1048–1051. doi:10.1175/1520-0426(2001)018<1048:WAAWPV>2.0.CO;2

Richards, C., D. Bourgault, P. S. Galbraith, A. Hay, and D. E. Kelley. 2013. Measurements of shoaling internal waves and

turbulence in an estuary. J. Geophys. Res. Oceans **118**: 273–286. doi:10.1029/2012JC008154

Scotti, A., and J. Pineda. 2007. Plankton accumulation and transport in propagating nonlinear internal fronts. J. Mar. Res. **65**: 117–145. doi:10.1357/002224007780388702

Shanks, A. L. 1983. Surface slicks associated with tidally forced internal waves may transport pelagic larvae of benthic invertebrates and fishes shoreward. Mar. Ecol. Prog. Ser. **13**: 311–315. doi:10.3354/meps013311

Shanks, A. L. 1995. Orientated swimming by megalopae of several eastern North Pacific crab species and its potential role in their onshore migration. J. Exp. Mar. Biol. Ecol. **186**: 1–16. doi:10.1016/0022-0981(94)00144-3

Shanks, A. L. 2009. Pelagic larval duration and dispersal distance revisited. Biol. Bull. **216**: 373–385. doi:10.2307/25548167

Shanks, A. L., and W. G. Wright. 1987. Internal-wave-mediated shoreward transport of cyprids, megalopae, and gammarids and correlated longshore differences in the settling rate of intertidal barnacles. J. Exp. Mar. Biol. Ecol. **114**: 1–13. doi:10.1016/0022-0981(87)90135-3

Shanks, A. L., and L. Brink. 2005. Upwelling, downwelling, and cross-shelf transport of bivalve larvae: Test of a hypothesis. Mar. Ecol. Prog. Ser. **302**: 1–12. doi:10.3354/meps302001

Shroyer, E. L., J. N. Moum, and J. D. Nash. 2009. Observations of polarity reversal in shoaling nonlinear internal waves. Am. Meteorol. Soc. **39**: 691–701. doi:10.1175/2008JPO3953.1

Shroyer, E. L., J. N. Moum, and J. D. Nash. 2010. Vertical heat flux and lateral mass transport in nonlinear internal waves. Geophys. Res. Lett. **37**: 1–5. doi:10.1029/2010GL042715

Shroyer, E. L., J. N. Moum, and J. D. Nash. 2011. Nonlinear internal waves over New Jersey's continental shelf. J. Geophys. Res. Oceans **116**: C03022. doi:10.1029/2010JC006332

Sinnett, G., F. Feddersen, A. J. Lucas, G. Pawlak, and E. Terrill. 2018. Observations of nonlinear internal wave run-up to the surfzone. J. Phys. Oceanogr. **48**: 531–554. doi:10.1175/JPO-D-17-0210.1

Smyth, W. D., J. N. Moum, and J. D. Nash. 2010. Narrowband oscillations in the upper equatorial ocean. Part II: Properties of shear instabilities. J. Phys. Oceanogr. **41**: 412–428. doi:10.1175/2010JPO4451.1

Stastna, M., and K. G. Lamb. 2002. Large fully nonlinear internal solitary waves: The effect of background current. Phys. Fluids **14**: 2987–2999. doi:10.1063/1.1496510

Tapia, F. J., and J. Pineda. 2007. Stage-specific distribution of barnacle larvae in nearshore waters: Potential for limited dispersal and high mortality rates. Mar. Ecol. Prog. Ser. **342**: 177–190. doi:10.3354/meps342177

Thorpe, S. A. 1968. On the shape of progressive internal waves. Philos. Trans. R. Soc. Lond. Ser. A Math. Phys. Sci. **263**: 563–614. doi:10.1098/rsta.1968.0033

van den Bremer, T. S., H. Yassin, and B. R. Sutherland. 2019. Lagrangian transport by vertically confined internal gravity wavepackets. J. Fluid Mech. **864**: 348–380. doi:10.1017/jfm.2019.30

Weidberg, N., C. Lobón, E. López, L. García Flórez, M. Fernández Rueda, J. Largier, and J. Acuña. 2014. Effect of nearshore surface slicks on meroplankton distribution: Role of larval behaviour. Mar. Ecol. Prog. Ser. **506**: 15–30. doi:10.3354/meps10777

Wunsch, C. 1971. Note on some Reynolds stress effects of internal waves on slopes. Deep-Sea Res. Oceanogr. Abstr. **18**: 583–591. doi:10.1016/0011-7471(71)90124-0

Zhang, S., M. H. Alford, and J. B. Mickett. 2015. Characteristics, generation and mass transport of nonlinear internal waves on the Washington continental shelf. J. Geophys. Res. Oceans **120**: 741–758. doi:10.1002/2014JC010393

Acknowledgments

We wish to thank two anonymous reviewers for feedback that greatly improved this manuscript, as well as Captain Ryan Hersey for operating the Kelona during field work, the SIO small boating program, Jennifer Mackinnon and Jonathan Nash for lending instruments, as well as Devin Ratelle, Andrew Mullen, Eric Orenstein, Brian Stock, and other volunteers for help in the field. We are also grateful to Ruth Musgrave for feedback throughout the project, Emily Shroyer for generously providing her KdV scripts, Amy Waterhouse and Arnaud Le Boyer for assistance with data processing, Jean-Michel Leconte and Jerry Molnar at RBR for live troubleshooting of the Wirewalker, as well as Dan Cayan and Douglas Alden for providing wind data from the Scripps Pier weather station. This material is based upon work supported by the National Science Foundation under Grant OCE-1459393. J.C.G. was also partially funded by an NSERC doctoral fellowship.

Conflict of Interest

None declared.

Submitted 18 February 2019
Revised 21 August 2019
Accepted 29 November 2019

Associate editor: Julia Mullarney